Composites: Part B 43 (2012) 2115–2124

Contents lists available at SciVerse ScienceDirect

Composites: Part B

journal homepage: www.elsevier.com/locate/compositesb

Tension–tension fatigue of hybrid composite rods

N.K. Kar *, Y. Hu, E. Barjasteh, S.R. Nutt

Gill Composites Center, Department of Chemical Engineering and Materials Science, Vivian Hall of Engineering 402, University of Southern California, Los Angeles, CA 90089, United States

ARTICLE INFO

Article history:
Received 3 August 2011
Accepted 11 March 2012
Available online 21 March 2012

Keywords:
A. Carbon fibers
A. Glass fibers
B. Fatigue
D. Acoustic emission

ABSTRACT

The tension–tension fatigue behavior was investigated for a hybrid composite rod comprised of a unidirectional carbon fiber core and a glass fiber shell. Fatigue tests were performed at three *R*-ratios and four maximum applied stress levels (MAS) while recording the secant modulus at each cycle, and acoustic emission (AE) sensors were employed to monitor the activation of fatigue mechanisms. Fatigue failure occurred when the composite rod was no longer able to support the applied cyclic load. For a MAS level of 70% of the ultimate tensile stress (UTS), composite rods tested at higher *R*-ratios showed AE activity through a larger percentage of fatigue life, but exhibited a greater resistance to fatigue failure, whereas samples cycled at lower *R*-ratios displayed AE activity only near the end of fatigue life, and showed a lower resistance to fatigue failure. The hybrid composite showed modes of progressive fatigue damage at high *R*-ratios and low strain amplitudes in the form of longitudinal splitting of the GF shell. In contrast, failure of the CF core was catastrophic and non-progressive. The fatigue resistance and damage mechanisms of the composite rod were dependent on the MAS level and *R*-ratio. Fatigue cracks initiated because of fretting between the GF shell and grip surface, which led to the observed longitudinal splitting of the GF shell. Fatigue damage occurred along the GF/CF interface where non-uniform strains developed because of the clamping force of the grip on the GF surface. At an *R*-ratio of 0.85, a fatigue stress of 70% UTS caused catastrophic fatigue failure, while at lower stresses, composite rods did not fail and withstood cyclic loads up to 1 million cycles. The research conducted is the first to investigate the degradation in fatigue performance arising from grip/composite rod interactions and suggests that the results from the study provide new information for composite materials in industries that utilize unidirectional composites in cylindrical form.

1. Introduction

Overhead conductors in use today consist of aluminum strands wrapped around a steel cable – the aluminum strands carry the current, and the steel cable supports the mechanical loads. The major factor limiting the capacity of such conductors is sag at high temperatures, which results from thermal expansion. To increase grid capacity, new conductors have been introduced that feature low sag at high temperatures. One such class of conductor is the high-voltage, composite-reinforced conductor (or CRC), in which the steel cable used in conventional conductors is replaced with a solid composite rod with low thermal expansion and high specific strength [1]. These conductors feature reduced line losses, lower operating temperatures for a given current, and higher strengths relative to conventional conductors. However, like conventional conductors, they are expected to deliver decades of service with little or no maintenance. Thus, long-term durability, which involves fatigue and aging phenomena, is an important issue that must be addressed before the technology can be widely deployed.

High-voltage transmission lines are suspended between lattice towers by tensioning during installation, and consequently CRCs will experience a static axial tensile stress. In addition, cyclic tensile stresses arise from dynamic service conditions that include wind, ambient temperature fluctuations, ice loading, and periods of high and low electricity demand. The long-term effects of such dynamic service conditions on the composite element of CRCs are not well understood. To date, no studies have been undertaken to characterize tension–tension fatigue mechanisms in composite rods developed for high voltage overhead transmission cables. However, studies have shown that GRP insulator rods are susceptible to brittle failure where multiple cracks can develop within fittings near rod/hardware interfaces [2,3]. Thus, for CRCs, the tension–tension fatigue behavior of the composite must be characterized and understood to accurately predict lifetime within the range of anticipated service conditions, to develop specifications for operating conditions, and to improve fatigue-resistant designs.

* Corresponding author. Tel.: +1 213 740 1634.
E-mail address: nkar@usc.edu (N.K. Kar).

1359-8368/$ - see front matter © 2012 Elsevier Ltd. All rights reserved.
http://dx.doi.org/10.1016/j.compositesb.2012.03.006

Fig. 1. CRC mechanical grip design.

The strong dependence of tensile fatigue behavior on composite structure has led to different, often contradictory conclusions. For example, some investigators have concluded that tension fatigue is fiber-dominated, and fatigue failure mechanisms are no different from those present in quasi-static loading [4,5]. Others, however, observed that higher modulus and strength fibers in the same epoxy matrix resulted in little improvement in fatigue behavior of unidirectional composites, and argued that fatigue depended more strongly on matrix strain [6]. These and similar discrepancies stem from factors such as the particular loading configuration, the fiber architecture, and the associated anisotropy.

Tension–tension fatigue testing of composites presents special challenges, some of which stem from the inherent anisotropy. This anisotropy generally causes cracks to grow more readily along fiber directions, which leads to splitting parallel to the fibers [7], often initiated at the grips. (Some test methods suggest gauge length failures are required to mimic damage that would occur in service conditions [8]). While failure initiation at grips is generally regarded as an unwanted artifact in lab tests, recent experience with overhead conductors has shown that failures of conventional overhead conductors typically originate at the node where the conductor cable is attached to the lattice tower [9,10]. While fatigue mechanisms for composites have been developed and explained for gauge-length-related failures, grip induced failures have largely been considered invalid for coupon testing [11], and have received little attention. Such observations underscore the importance of stress concentrations associated with gripping, both in service and in fatigue testing. This is particularly critical for unidirectional composite rods, such as those used in CRCs. Fig. 1 shows the design of a new self-tightening, collet fixture used to grip the composite core in service. As the axial tensile load increases, the compressive pressure exerted on the composite rod increases, preventing slip. Because the transverse strength properties of unidirectional FRCs are much lower than longitudinal values, failure mechanisms can originate and grow due to stress variations where transverse loads are the greatest.

The objective of this study is to characterize the effect of stress concentrations induced by hardware fixtures on tensile fatigue life and failure mechanisms of a hybrid composite rod similar to those designed for CRCs. Tension–tension fatigue tests were conducted using collet grip fixtures similar to those designed for attaching CRCs to splices and dead ends. Experiments using load-control fatigue tests suggest fatigue failure occurs when the residual strength of the composite reaches the cyclic stress, and catastrophic failure ensues [12,13]. S–N curves are developed to illustrate the lifetime of the composite under varying load conditions, and failure modes are observed and characterized using microscopy, acoustic emission and finite element analysis.

2. Experiments

2.1. Materials

Unidirectional hybrid composite rods were acquired for fatigue testing (Composite Technology Corporation, Irvine, CA). Each rod consisted of a unidirectional carbon fiber core (CF) surrounded by a glass fiber shell (GF), and an epoxy matrix, as described elsewhere [14,15]. The CF core and GF shell regions comprised 44 and 56% of the composite volume, and the carbon fiber and glass fiber volume fractions for core and shell were ~69%. The epoxy matrix was formulated for a high glass transition temperature (T_g = 205 °C). Test specimens were cut to lengths of 610 mm from production composite rods with a ~6 mm diameter.

2.2. Stress state and fatigue tests

Static tensile tests and tension–tension fatigue tests were conducted using a hydraulic load frame (Instron 8500) with a 100 kN load cell. Static tensile tests were conducted on specimens using custom made tensile test fixtures in accordance with ASTM D3916. The average ultimate tensile strength (UTS) was 2.24 GPa, and catastrophic failure occurred when the composite strain reached the carbon fiber failure strain of ~2%. Load control fatigue tests were performed at three *R*-ratios (minimum stress/maximum stress) ranging from 0.5 to 0.85 at a fixed frequency of 5 Hz following ASTM D 3479. The maximum applied stress (MAS), ranged from 50% to 80% of the UTS.

A set of mechanical grips similar to those used in service (Fig. 1) were designed and fabricated for conducting tension–tension fatigue tests. As shown in Fig. 2, the grips employ a long collet that exerts a radial clamping force that increases as the tensile load is applied. The collet grip design utilizes two concave anvils to ensure that the gripping pressure applied to the surface of the rod is sufficient to prevent slip. This leads to a variation in radial displacements, with the maximum displacement occurring on the GF shell surface in regions farthest from the gap spacing, indicated in Fig. 2. The friction force between the grip and the rod increases with radial displacement, which resists slippage under higher axial loads. The maximum radial displacement (u_{max}) is a function of the applied tensile displacement ($\varepsilon_z L$) and the grip angle (α):

$$u_{max} = \varepsilon_z L \tan\alpha \tag{1}$$

To verify the accuracy of the estimated maximum radial displacement, the gap spacing was measured as a function of applied axial load and is shown in Table 1, compared with estimated values. The corresponding maximum radial load that results from the maximum radial displacement was determined by compressing the rod surface using two concave anvils with the same geometry as the grips.

2.3. Finite element analysis

Finite element analysis (FEA) was performed to determine the stress distribution within the composite rod subject to an imposed radial displacement and an applied axial load. The composite rod properties were taken to be transversely isotropic [3], (where r and θ are the transverse directions) and are described in Table 2. A 3D model was developed using constituent properties, and the specimen was modeled to represent the geometrical features of the test setup, using exact dimensions from the experiment. Load and boundary conditions were simulated with commercially available FEA software (ABAQUS and SolidWorks FEA Simulation Package) using 183,000 elements with a four-node, bilinear, axisymmetric, quadrilateral element (CAX4R, commonly used in ABAQUS) in the 2D model, and 47,995 C3D8R elements in the 3D model. The analysis involved two load steps. In the first step, a radial displacement was applied, and in the second step, an axial load was applied. The analysis was performed to determine the stress distribution resulting from the grip design.

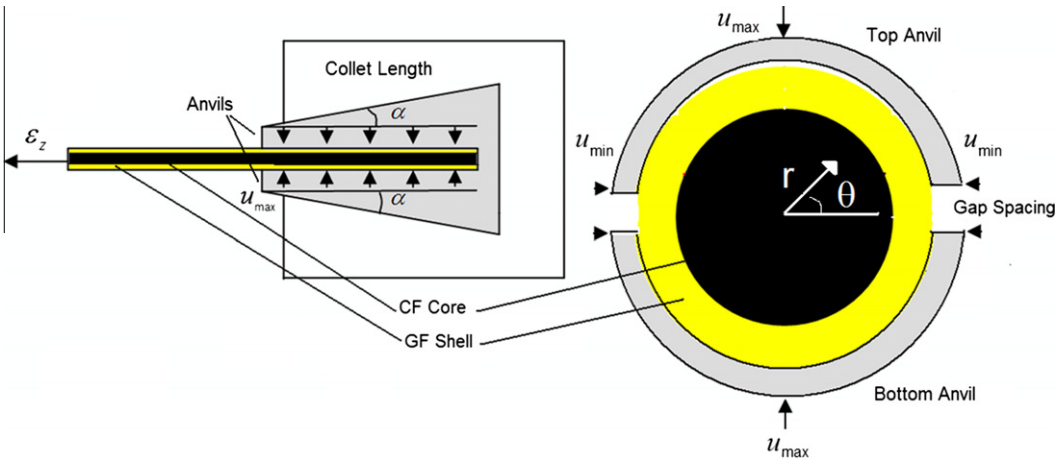

Fig. 2. 2D diagram indicating relationship between longitudinal extension on radial compression, and a cross sectional view of CF core and GF shell under mechanical grip.

Table 1
Radial displacements as a function of UTS.

Axial load	Calculated max radial displacement (mm)	Measured max radial displacement (mm)
50% of UTS	0.18	0.20
60% of UTS	0.21	0.23
70% of UTS	0.25	0.24
80% of UTS	0.28	0.24

Table 2
Material properties in longitudinal and transverse directions.

	GF/epoxy	CF/epoxy
E_z (GPa)	47	139.4
$E_r = E_\theta$ (GPa)	10.8	7
$\nu_{zr} = \nu_{z\theta} = \nu_{r\theta}$	0.214	0.27
$G_{zr} = G_{z\theta}$ (GPa)	6.3	2.9

3. Monitoring stiffness and acoustic emission

3.1. Definition of secant modulus

Stiffness measurements were performed during fatigue tests as a non-destructive means to quantitatively monitor the accumulation of damage. During load-controlled fatigue tests, the maximum and minimum loads during each cycle were recorded, as well as the elongation. The secant structural modulus (*SM*) was calculated from:

$$SM(N) = \frac{F_{max}(N) - F_{min}(N)}{l_{max}(N) - l_{min}(N)} \quad (2)$$

where l is the displacement and the subscripts *max* and *min* are the maximum and minimum values of the load or displacement for cycle N [16]. The normalized *SM* was calculated by dividing $SM(N)$ by $SM(0)$, which was recorded on the first cycle of each test. For a given *R*-ratio and stress level, catastrophic failure occurred when the applied stress reached the residual strength of the composite. The number of cycles to failure (N_f) was then determined. Specimens that exceeded 1 million cycles without failure were considered run-outs.

3.2. Acoustic emission

The acoustic emission (AE) technique was used as an in situ, qualitative method to detect different modes of fatigue damage. In the present work, two acoustic emission resonance transducers (300 kHz Micro 30, Physical Acoustics PCI-2) were placed on each grip edge to detect damage events. A graphical amplitude filter was employed to exclude noise caused by the hydraulic pump. The transducer positioned closer to the hydraulic piston (attached to bottom grip) detected significant noise from the pump and was in constant cyclic motion, which compromised the ability to locate AE sources. The transducer farthest from the pump (attached to the stationary top grip) also detected hydraulic noise, but the amplitude of this signal was attenuated, allowing the transducer to detect a wider range of amplitudes caused by damage events. Thus, only data collected from this sensor was used. In fiber reinforced composites, a damage event releases energy and produces a transient elastic wave [17]. The most important AE parameters for burst type signals are counts, amplitude, duration and absolute energy [18]. The AE response was continuously monitored during fatigue tests, and detected AE decibel hit signals were correlated with fatigue failure mechanisms.

4. Results and discussion

4.1. Effect of R-ratio on stiffness and S–N diagram

The tension–tension fatigue response for the three *R*-ratios and four MAS levels is shown in Fig. 3, where the normalized *SM* is plotted against the number of cycles. At all *R*-ratios, increasing the MAS caused the number of cycles to failure to decrease. Increasing the *R*-ratio caused the fatigue stress (taken as the MAS to cause catastrophic fatigue failure) to increase. At $R = 0.50$, catastrophic failure occurred for all four MAS levels, while at $R = 0.68$, failure occurred only for MAS $\geqslant$60% UTS, and at $R = 0.85$, failure occurred for MAS stress $\geqslant$70% UTS. All *R*-ratios show the same trend in modulus loss – the *SM* remains constant for the initial portion of the fatigue life until damage events cause abrupt *SM* drops, with ensuing catastrophic failure. The first drop in *SM* indicated that composite damage had occurred, but was still able to carry the cyclic load. The applied cyclic load was redistributed and a slightly lower, steady *SM* was maintained temporarily while the load cycles

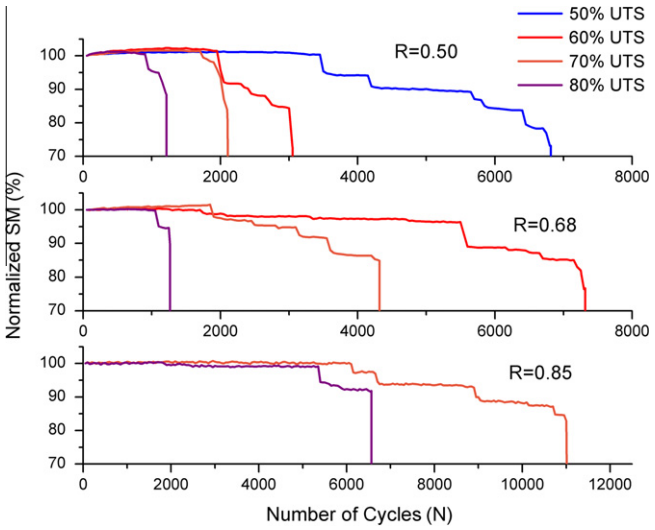

Fig. 3. *SM* loss at three *R*-ratios and four stress levels.

continued. Subsequent modulus drops transpire, with plateaus at lower *SM* values. Eventually the fatigue damage saturated, and catastrophic failure occurred, manifested as a precipitous drop in *SM*, taken as the fatigue life (N_f). Fig. 3 also shows that for any fixed *R*-ratio, a shift in material behavior occurs as the MAS level increases. In particular, for small MAS values, multiple small decrements in *SM* are observed, while for larger MAS values, the *SM* remains nearly constant over most of the fatigue life, and rapid failure and modulus loss occurs near the end of fatigue life. The tension–tension fatigue behavior of the hybrid composite rod differs from that of typical composite laminates, where investigators normally observe a sigmoidal response of stiffness deterioration earlier in life, followed by a steady loss in stiffness and eventual catastrophic failure [19].

The S–N curves in Fig. 4 show the effects of the MAS level and *R*-ratio on fatigue life. Increasing the MAS level (for any *R*-ratio) reduced fatigue life. The S–N curves show that for a fixed MAS level, lower *R*-ratios resulted in a shorter fatigue life. At 80% UTS, the *R*-ratio had little effect on fatigue life, as N_f varied slightly between 1000 and 1500 cycles for *R*-ratios 0.50 and 0.68, and increased to 7000 cycles for $R = 0.85$. However, at a MAS level of 60% UTS, the fatigue life increased from ~3000 (for $R = 0.50$) to 15000 cycles (for $R = 0.68$) and was beyond 1 million cycles for $R = 0.85$. Thus, the effect of *R*-ratio on fatigue life was more pronounced at lower stress levels.

The effect of frequency on fatigue life was also investigated. Variation in frequency can affect both specimen temperature and strain rate. Research has shown CF composites are relatively insensitive to strain rate in the longitudinal direction, although the mechanical properties of GF composites show stronger rate dependence [20]. Reducing the cycle frequency to 2.5 Hz caused no significant deviation in fatigue life, as shown in Fig. 4, indicating that the load frequency had little effect for this study. Also, because the frequencies used were relatively low, sample heating was negligible.

The testing of multiple samples resulted in statistical scatter in fatigue life, and a regression model was used to relate the fatigue life to the stress level, as shown in the power-law relationship below:

$$N_f = A\left(\frac{\sigma}{\sigma_{UTS}}\right)^B \tag{3}$$

where *A* and *B* are material parameters. The data conform to this relationship, as shown in Fig. 4, indicating the existence of an endurance limit, below which fatigue failure does not occur. As shown in the plots, fatigue life is affected by the *R*-ratio. This is particularly apparent when observing the log–log relationship at the two lower *R*-ratios ($R = 0.5$ and $R = 0.68$):

$$\begin{aligned} \log(N_f^{R=0.50}) &= 15.843 - 6.85\log\left(\tfrac{\sigma}{\sigma_{UTS}}\right) \quad r^2 = 0.89 \\ \log(N_f^{R=0.68}) &= 20.45 - 9.09\log\left(\tfrac{\sigma}{\sigma_{UTS}}\right) \quad r^2 = 0.97 \end{aligned} \tag{4}$$

The high correlation coefficients in Eq. (4) ($r^2 = 0.89$ and 0.97) indicate a strong relationship between fatigue life and stress level. On the other hand, the effect of the *R*-ratio is reflected in the prelogarithmic term (equal to *B* in Eq. (3)). This term, effectively the value of the slope in Eq. (4), quantitatively relates the effect of the *R*-ratio on fatigue life, and is an indicator of fatigue resistance. For example, a slope of −9.09 compared to −6.85 indicates that a longer fatigue life is predicted at larger *R*-ratios and lower MAS levels. Thus, the hybrid composite is more fatigue-resistant at higher *R*-ratios, which is a result of lower cyclic strain amplitudes at high *R*-ratios.

The initial strain amplitudes (within the gauge length) of the composite at the three *R*-ratios and four MAS levels are shown in Table 3. The table indicates that at $R = 0.85$, the cyclic strain amplitude varied between 0.17% and 0.27%, the lowest range of strain values of all the three *R*-ratios regardless of stress level. Note that

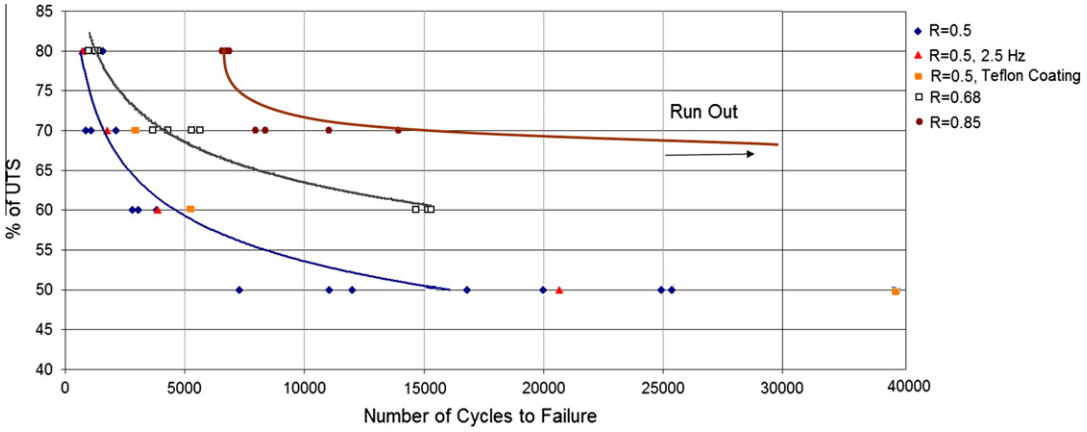

Fig. 4. S–N curve at 3 *R*-ratios showing endurance behavior.

Table 3
Strain amplitude at three *R*-ratios.

	R = 0.5 strain amplitude (%)	*R* = 0.68 strain amplitude (%)	*R* = 0.85 strain amplitude (%)
50% of UTS	0.56	0.36	0.17
60% of UTS	0.67	0.43	0.20
70% of UTS	0.78	0.50	0.24
80% of UTS	0.90	0.57	0.27

CFRPs reportedly do not experience fatigue damage when cyclic strain amplitudes are sufficiently low [8]. Thus, the low strain amplitudes at $R = 0.85$ are an indication of why composite rods cycled at MAS levels of 50% UTS and 60% UTS survived over 1 million cycles without catastrophic failure. Although fatigue damage occurred in the GF shell, the cyclic applied load was supported primarily by the CF core, which showed no evidence of fatigue damage at low strain amplitudes.

4.2. Acoustic emission output

The AE amplitude response is shown concurrently with the *SM* loss in Fig. 5 for a fixed MAS level of 70% UTS at the three *R*-ratios. Each red dot represents a single hit, corresponding to the detection of an AE signal arising from an active damage mode. The data in Fig. 5 show that during the early stage of tension–tension fatigue, the *SM* was nearly constant, and no AE signals were detected, indicating negligible damage. The end of the early stage was marked by a sharp drop in the secant modulus, accompanied by a rise in the value and number of AE hits, indicating the onset of a fatigue damage mechanism. The audible damage events occurred within the GF shell and originated near the grip/gauge length transition

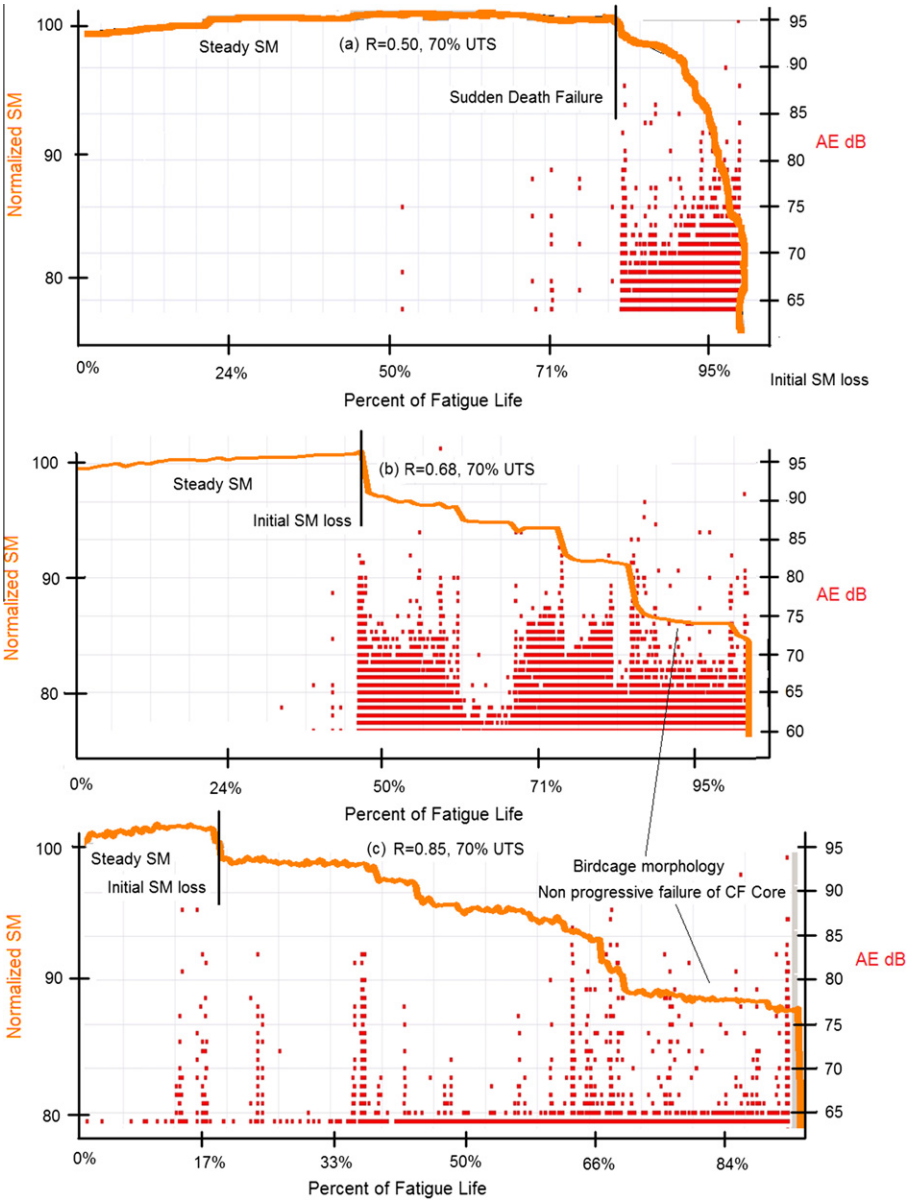

Fig. 5. AE hits and damage versus fatigue life for a maximum stress level of 70% UTS at three *R*-ratios.

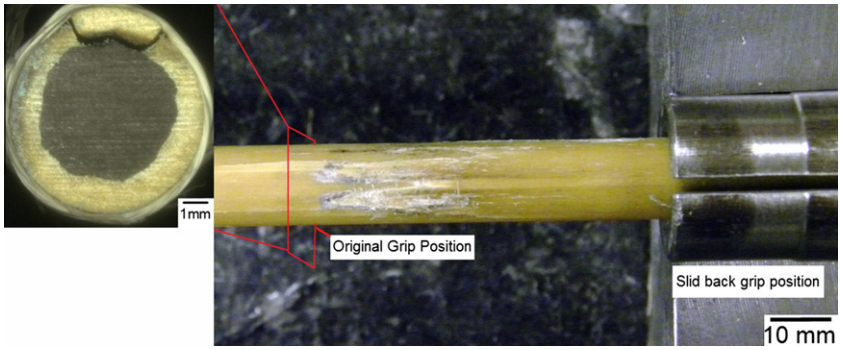

Fig. 6. Damage initiates as cracks in the GF shell near rod/grip zone along the CF/GF interface.

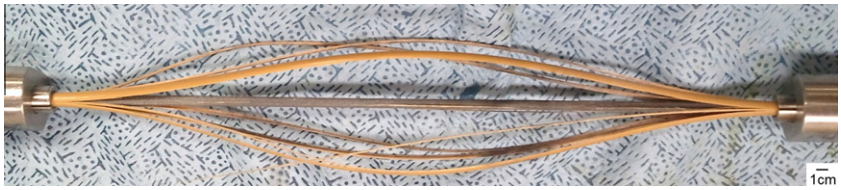

Fig. 7. Complete GF/CF separation termed bird caging.

region, shown in Fig. 6. Fretting fatigue damage at the GF surface, caused by the collet fixture, led to the formation and propagation of a radial crack through the GF shell, which was subsequently deflected at the GF/CF interface and propagated as a longitudinal crack along the gauge length (see micrograph in Fig. 6). This pattern of initial failure manifested as bundles of GF fibers separating from the GF/CF interface, as shown in Fig. 6.

Prominent drops and plateaus in *SM* occur after the initial *SM* loss, as shown in Fig. 5b and c. In particular, for *R* ratios of 0.68 and 0.85, progressive damage occurs within the GF shell, where each drop in *SM* corresponds to an AE amplitude peak. The damage mode was progressive because each *SM* drop was correlated with a macroscopic damage event accompanied by a burst of AE signals. The peaks in AE amplitude in Fig. 5b and c represent progressive longitudinal splitting of the GF shell, and are characterized by a high amplitude output range of 80–95 dB. Each longitudinal split in the GF shell originated within a grip and propagated along the gauge length, both as a radial crack in the GF shell and a longitudinal crack at the GF/CF interface. The fatigue resistance of unidirectional composites reportedly depends on the susceptibility to longitudinal splitting [21]. In the present investigation, the GF shell showed clear signs of this mechanism. These wedge-shaped GF bundle cracks grew parallel to the fiber direction, and were responsible for the progressive step-wise losses in the *SM*.

Two mechanisms of fretting damage in the GF shell were apparent during tension–tension fatigue tests, and these were detectable only by analyzing the AE data and observing the fracture surfaces. As the GF shell debonded from the CF core, broken sections of the GF shell continued to slide and abrade unbroken fibers, a phenomenon that was both visible and audible. Signs of fretting damage were also evident along the surface of the GF shell that was in contact with the collet grip (Fig. 6). Fretting fatigue damage was manifested in the AE data as signals of repeated low-AE-amplitude (60–70 dB, Fig. 5). These signals increased in frequency with fatigue life, demonstrating that fretting fatigue of the GF shell was an important damage mechanism contributing to fatigue failure. Kim and Ebert [22] determined that the surface integrity of the glass fiber was the most critical factor limiting the fatigue life of a GF composite, and surface integrity can be compromised during fatigue

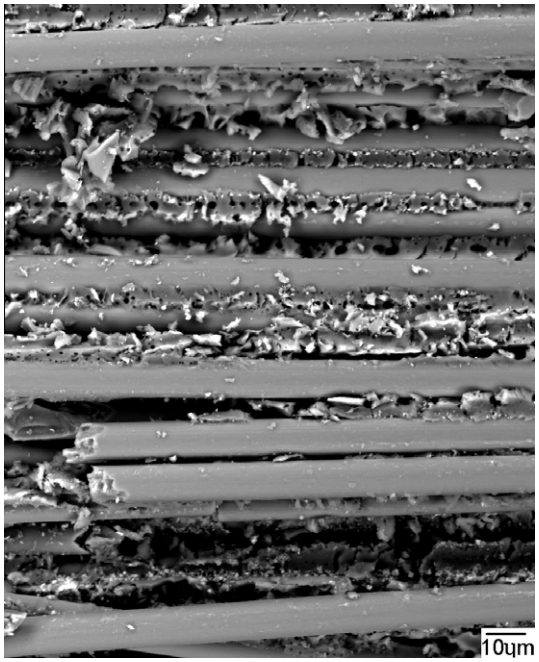

Fig. 8. Catastrophic failure of CFs at end of fatigue life.

loading because of fiber–fiber contact (fretting type damage) produced during high-amplitude stress cycling [23].

The tension–tension fatigue behavior of the hybrid composite led to complete failure of the CF core because of a transition in damage mechanisms and load sharing behavior. The growth of multiple longitudinal cracks (along the CF/GF interface) led to a 10–20% loss in *SM* after ~70% of the fatigue life, (see arrow in Fig. 5b and c). Eventually, these cracks led to complete separation of the GF shell from the carbon fiber core, corresponding to the lowest *SM* plateau prior to catastrophic failure. This resulted in a bird cage morphology, as shown in Fig. 7. At this stage, (complete shell/core separation), the CF core supported all of the applied

cyclic loads. Fig. 5b and c show that after the bird-caging effect, the *SM* remained constant until final failure, and there were no prominent peaks in AE signals until the CF core failed catastrophically.

The failure-causing damage to the CF core was characterized by multiple fiber breaks and fiber/matrix interface separation, as shown in Fig. 8. While some of the outermost fibers of the CF core detached with portions of the GF shell during bird-caging, the bulk of the CFs did not separate, and the majority of the core remained intact until catastrophic failure occurred. There was no evidence of progressive fatigue damage in the CF core, and the fracture surfaces were similar to the failures observed in tensile strength tests. Supporting this contention, the normalized *SM* remained nearly constant during the final 20–30% of fatigue life (at 80–90% of *SM*), a period during which the load was supported solely by the CF core (see Fig. 5b and c). During this period, the number of random fiber breaks increased with the number of cycles, but because the *SM* remained constant, the damage was negligible and the failure of the CF core was non-progressive. Eventually, the distribution of broken carbon fibers reached a critical stage at which point catastrophic failure occurred, corresponding to a final peak in AE amplitude (near 95 dB) and a drop in *SM* to zero.

4.3. Failure mechanisms

Fig. 3 shows that the hybrid composite undergoes a transition from continuous degradation of the *SM* to a sudden-death failure with increasing MAS levels and strain amplitudes. In previous fatigue studies, progressive damage mechanisms were responsible for the steady degradation of the *SM* where a zone of damage was traced, while non-progressive damage mechanisms were indicated by a sudden-death behavior of the *SM* [24,25]. Progressive damage mechanisms in composites are matrix-dependent failure modes, and typically start within the matrix and propagate along the fiber/matrix interface. In contrast, non-progressive damage mechanisms are fiber-dominated failure modes, and are catastrophic in nature. Table 3 shows that lower *R*-ratios corresponded to higher initial strain amplitudes, ranging from 0.17% to 0.9% within the gauge length. The strain amplitude was 0.78% for $R = 0.50$, and was lowest (0.24%) for $R = 0.85$, at a MAS of 70% UTS.

The high strain amplitude of 0.78% led to sudden-death failure of the entire hybrid composite, as shown in Fig. 5a. This trend is consistent with Talreja's investigations showing that higher maximum strain amplitudes corresponded to non-progressive catastrophic failure [26]. In Fig. 5a, AE activity occurred only in the last 20% of the fatigue life, while at higher *R*-ratios, AE activity initiated within the first 20–50% of life, and was present throughout, as shown in Fig. 5b and c. This continuous AE activity throughout most of the fatigue life reflects a progressive damage mechanism. The scaled AE activity early in fatigue life was an indication that increasing the *R*-ratio led to the activation of progressive damage mechanisms, at lower strain amplitudes. Lower MAS levels and higher *R*-ratios produced lower strain amplitudes, leading to early, progressive damage of the GF shell and higher fatigue lives. On the other hand, higher MAS levels and lower *R*-ratios produced higher strain amplitudes, leading to non-progressive, sudden-death failure of the entire hybrid composite and shorter fatigue lives.

4.4. Effect of stress distribution on crack initiation

The stress distribution in the composite rod during tension–tension fatigue tests affected the observed fatigue mechanisms. Portnov and Bakis [27] showed that for all types of methods used to grip and pull pultruded composite rods; the tensile load is maintained by the shear stress acting on the surface of the rod within the grips. Near the grip edges, tensile and hoop stresses are concentrated, and are related to the value and distribution of the surface shear stress. In the case of flat laminate coupons, stress concentrations within grips are commonly mitigated by the use of tabs, although conventional tabs cannot be deployed with cylindrical rods.

Stress concentrations within the grip were a function of the distribution of radial displacements, which were determined by finite element (FE) analysis. Fig. 9a shows the distribution of radial displacements at 50% UTS (axial load) under an imposed radial displacement in a 3D FE model. The radial displacements were slightly non-uniform as a result of the slit spacing inherent in the collet grip design (see Fig. 2). The analysis revealed that the greatest radial displacements occurred near the top and bottom of the grip (u_{max} in Fig. 2), where the greatest radial loads occurred. These regions experienced minimal fretting damage because the high radial displacements prevented axial displacements (slippage). Large radial displacements can cause high transverse compressive stresses to develop that can crush composites [28]. Thus, radial displacements ideally should be sufficiently large to prevent fretting and slip, but small enough to prevent compressive overload and crushing (not observed in this study). The smallest radial displacements (u_{min} in Fig. 9a) occur near the collet slit where the two concave anvils of the collet meet. This analysis is consistent with Fig. 6, which shows the formation of fatigue cracks in regions where radial displacements are minimal and where the sharp edges of the collet exist. These sharp edges created grooves on the GF surface (see Fig. 6), and allowed the composite rod to slip and fret during tensile fatigue.

The effects of the radial displacements on the tensile stress distribution in the composite rod are shown in Fig. 9b and c. Fig. 9b shows the 3D distribution of stress within the gauge length, and near the grip edge (MAS = 50% UTS) in the plane where the greatest radial displacement occurred. The stress distribution along the gauge length is uniform within the CF core (1.7 GPa) and the GF shell (0.57 GPa). However, the discontinuity in stress arises at the core–shell interface because of the abrupt modulus mismatch between the two material systems (see Table 1). The longitudinal composite stress (σ_c) can be evaluated as:

$$\sigma_c = E_c\varepsilon_c = (E_{GF}V_{GF} + E_{CF}V_{CF})\varepsilon_c \tag{5}$$

where subscripts GF and CF represent the homogenized material systems (fiber and matrix), and an isostrain condition is assumed within the gauge length region. Using Eq. (5) and the longitudinal elastic constants shown in Table 1, one can show that the CF core bears 70–80% of the applied load, while the GF shell bears the remaining 20–30% (dependent on the CF core/ GF shell diameter). The distribution of tensile stress becomes non-uniform near the grip entrance in both material systems, where non-uniform radial displacements (and loads) are introduced. Fig. 9b and c show that a transition from longitudinal tension (caused by surface shear stresses) to longitudinal and transverse compression (caused by the radial load) occurs deeper within the grip. The plane in which the radial displacement is greatest causes the maximum longitudinal tensile stress (in both the GF shell and CF core) to increase to ~0.8 GPa and ~1.83 GPa, respectively. Fig. 9c shows that in the plane with the lowest radial displacement, the stress concentration region was smaller, indicating that lower radial displacements reduced stress concentrations.

The results show that during tension–tension fatigue, the non-uniform distribution of longitudinal stress near the grip ends caused the composite to experience larger cyclic stresses within the collet grip than within the gauge length. The concentrated cyclic stresses within the grip increased the probability of initiating and propagating cracks during tension–tension fatigue. Table 2 indicates that higher tensile loads generate larger radial displacements which are necessary to prevent slip, but increases the severity of stress concentrations. Thus, the probability of crack

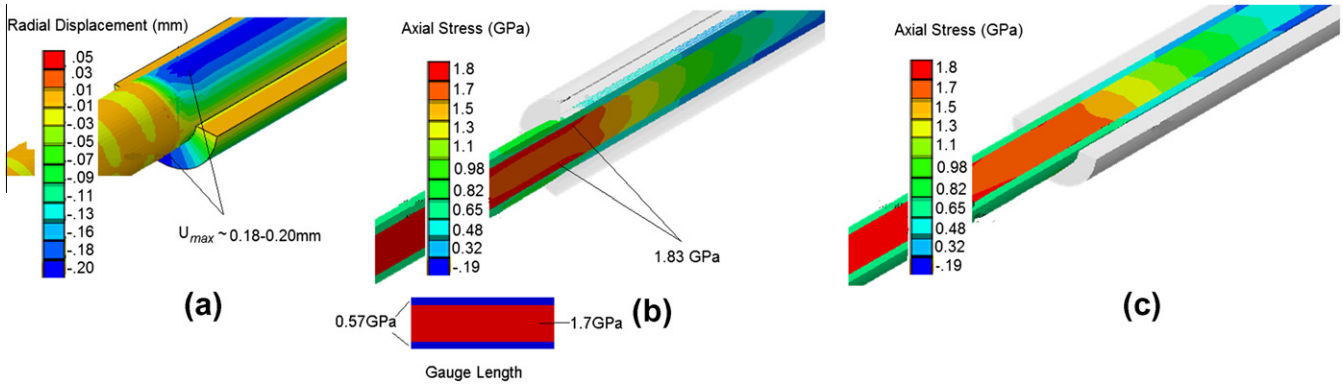

Fig. 9. (a) Non-uniform radial displacement of grip, (b) stress distribution in plane with maximum radial displacement and (c) stress distribution in plane with minimum radial displacement.

propagation increases at higher MAS levels because of the greater radial displacement required to prevent slip within the grips.

4.5. Interfacial separation

Crack growth parallel to the fiber direction and along interfaces occurred during tension–tension fatigue of the hybrid composite rod. Cracks grew and propagated along the GF/CF interface into the gauge length, and led to complete separation of the GF/CF systems. The interface between two materials is often weak relative to fiber strengths, providing preferred pathways for crack propagation [29]. Multiple factors can cause materials to separate along interfaces, one of which is the abrupt change in elastic modulus between the CF and GF systems. In the present case, the modulus mismatch caused a discontinuity of stress to arise at the interface that was amplified within the collet grip. In this region, shear stresses can also develop if there is relative motion between the two material systems.

Fig. 10a shows the longitudinal strain distribution within the gauge length at 50% UTS, where an isostrain condition exists at 1.1% strain. During tension fatigue, the composite was initially cycled between two positions where the two fiber types and the matrix reached uniform strains (within the gauge length). Fig. 10b shows that the axial strain increases along the GF/CF interface near the grip entrance, rising to a maximum of 1.4% in the GF shell. This distribution constitutes a strain gradient within the matrix near the GF/CF interface. During tension–tension fatigue, the strain gradient along the interface produced a shearing effect in the matrix and caused separation of the GF shell from the CF core, resulting in relative sliding between the CF core and the GF shell. These observations are consistent with previous observations of fatigue cracks initiating in regions of high matrix strain and propagating along stress concentration sites [18].

4.6. Design considerations

To mitigate the issues of high interfacial stress concentrations and fretting fatigue within the grip, a new design consideration was proposed. The addition of a thin sleeve, (25 mm in length) near the grip/gauge length interface is contemplated to reduce the friction coefficient and the maximum radial displacement (within the region). The radial displacement was reduced from 0.18 mm to 0.10 mm and the friction coefficient was reduced by 20% in the 25 mm length region to hypothetically model the effect of a sleeve. The effect of such a sleeve on the stress distribution in the rod was analyzed using a 2D FE model, and the results are shown in Fig. 11. The simulation shows that stress concentrations were reduced by ~10% in both the GF and CF systems. The corresponding stress states in the 2D model are similar to those determined by the 3D model. If similar sleeves were implemented in service, they would reduce stress concentrations in the grip while allowing a lower more uniform distribution of radial displacement. This sleeve would also protect the GF shell from fretting fatigue damage caused by the sharp grooves in the grip design.

To validate the model predictions and determine the effect of a protective sleeve on fatigue life, a PTFE (polytetrafluoroethylene) film was wrapped on the composite rod within the grip/gauge length transition region. As shown in Fig. 4, at $R = 0.50$ and 50% UTS, the fatigue life more than doubled after application of the PTFE film, increasing from an average of 16,872 ± 7300 (no coating)

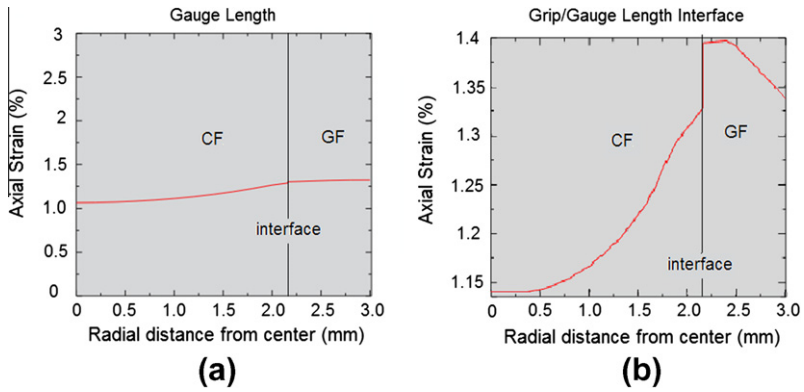

Fig. 10. (a) Axial strain at 50% UTS along gauge length and (b) non-uniform axial strain at interface.

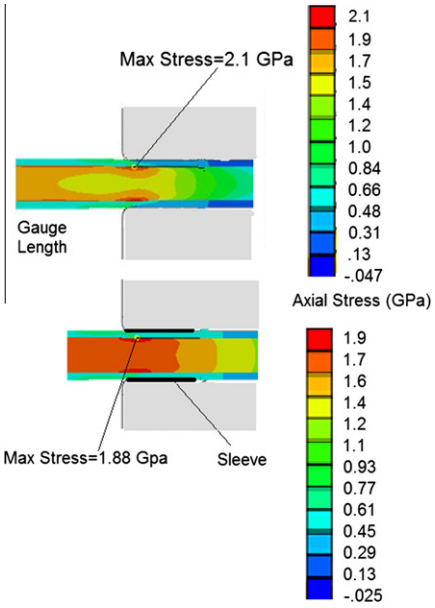

Fig. 11. Tensile stress distribution with and without sleeve.

to 38,194 cycles. At 60 and 70% UTS, the fatigue life with the PTFE sleeve was 5433 and 2835 cycles, both nearly double the average fatigue life of control samples at the respective stress levels. A statistical analysis of the fatigue life distributions of sleeveless samples indicates that only a 1% probability of the population would reach such high fatigue lives. Observations of the crack initiation sites revealed that the sleeve delayed the onset of GF shell fretting cracks, acting as a protective sliding contact. Thus, the sleeve strongly affected the fatigue life and similar measures are expected to reduce fatigue cracks and extend fatigue life for hybrid composite rods in service applications.

5. Conclusions

The tension–tension fatigue behavior of a hybrid composite rod comprised of unidirectional carbon and glass fibers was investigated. The technique used to grip the composite influenced the observed fatigue behavior and damage mechanisms, and the stress distributions showed that regions within the collet grip having the greatest radial displacement experienced the greatest tensile stresses. Cracks initiated in regions with low radial displacements, where the sharp collet edges rubbed against the GF shell. Longitudinal cracks grew along the GF/CF interface until complete shell/core separation occurred. Lower *R*-ratios and higher MAS levels led to shorter fatigue lives because of the transition from progressive fatigue failure to non-progressive fatigue failure.

Modifications to the grip design were considered that would increase the overall durability of the composite component in CRCs under both laboratory conditions and service conditions. In service, conductors are expected to be tensioned to a maximum stress level of 25% UTS, much lower than the levels of 50–80% UTS used for fatigue tests described here. However, overstressed conditions routinely arise in service, and it is important to understand the effects of stress concentrations that will develop at dead-ends and splices where hardware is used to attach the conductor to support towers. The results of this study suggest that while the gripping technique is adequate to support the appropriate loads, stress concentrations arise near the grip edges, where fretting damage can be induced under cyclic loading. FEA simulations and trial experiments showed that a thin protective sleeve over the composite rod would reduce fretting and stress concentrations, and thus extend fatigue life.

The hybrid composite design exhibited robust fatigue behavior – rods supported high cyclic loading levels (60% UTS) for more than 1 million cycles. The fatigue resistance stems from the fact that damage was confined to the GF shell, while the major load-bearing component (the CF core) was largely immune to fatigue damage. Improvements in interfacial adhesion or a gradual transition zone between CF and GF components (as opposed to the abrupt material transition) could delay or prevent core–shell debonding (as well as the attendant bird-caging phenomenon), and these approaches are presently being explored. With the advent of new conductor designs such as the CRCs, fatigue damage modes must be analyzed and understood to prevent failure from occurring in service. Because most service-related material failures are caused by some form of fatigue and service lives for infrastructure applications typically span multiple decades, composite designs for applications like CRCs will require consideration of fatigue resistance. Furthermore, CRCs will be deployed in outdoor environments with minimal protection, and thus aging factors such as thermal oxidation and degradation and moisture uptake will further limit fatigue life of composites. These aging factors have been studied for CRC composites [14,15,18], although the interaction of their combined effects on long-term durability has not yet been considered. Accounting for such interactions, which are undoubtedly complex, will be necessary to develop a realistic and accurate model for CRC lifetime prediction.

Acknowledgments

Composite Technology Corporation is gratefully acknowledged for the supply of samples and test fixtures. The authors also acknowledge Ryan van Schilfgaarde, Chris Fisher of USC and Dr. Ron Miller of Physical Acoustics Corp. for their advice and support.

References

[1] Alawar A, Bosze EJ, Nutt SR. A composite core conductor for low sag at high temperatures. IEEE Trans Power Deliv 2005;20(3):2193–9.
[2] Bansal A, Schubert A, Balakrishnan MV, Kumosa M. Finite element analysis of substation composite insulators. Compos Sci Technol 1995;55:375–89.
[3] Lanteigne J, De Tourreil C. The mechanical performance of GRP used in electrical suspension insulators. Compos Math Appl 1985;11(10):1007–21.
[4] Keller T, Tirelli T, Zhou A. Tensile fatigue performance of pultruded glass fiber reinforced polymer profiles. Compos Struct 2005;68:235–45.
[5] Zhang Y, Vassilopoulos AP, Keller T. Stiffness degradation and fatigue life prediction of adhesively-bonded joints for fiber-reinforced polymer composites. Int J Fatigue 2008;30:813–1820.
[6] Curtis PT. The fatigue behaviour of fibrous composite materials. J Strain Anal 1989;24(4).
[7] Meziere Y, Bunsell AR, Favry Y, Teissedre JC, Do AT. Large strain cyclic fatigue testing of unidirectional carbon fibre reinforced epoxy resin. Composites Part A 2005;36:1627–36.
[8] ASTM D 3479. Standard test method for tension–tension fatigue of polymer matrix composite materials. ASTM; 2007.
[9] Brunair RM, Ramey GE, Duncan III RR. An experimental evaluation of S–N curves and validity of miner's cumulative damage hypothesis for an ACSR conductor. IEEE Trans Power Deliv 1988;3(3).
[10] Cardou A, Cloutier L, Lanteigne J, M'Boup P. Fatigue strength characterization of ACSR electrical conductors at suspension clamps. Elect Power Syst Res 1990;19:61–71.
[11] Hodgkinson JM. Mechanical testing of advanced composites. CRC Press; 2000. 65.
[12] Kawai M. A phenomenological model for off-axis fatigue behavior of unidirectional polymer matrix composites under different stress ratios. Composites: Part A 2004;35:955–63.
[13] Epaarachchi JA, Clausen PD. An empirical model for fatigue behavior prediction of glass fibre-reinforced plastic composites for various stress ratios and test frequencies. Composites: Part A 2003;34:313–26.
[14] Tsai YI, Bosze EJ, Barjasteh E, Nutt SR. Influence of hygrothermal environment on thermal and mechanical properties of carbon fiber/fiber glass composites. Compos Sci Technol 2009;69(3–4):432–7.

[15] Barjasteh E, Bosze EJ, Nutt SR. Thermal aging of fiberglass/carbon-fiber hybrid composites. Composites Part: A 2009;40(12):2038–45.
[16] Zhang Y, Vassilopoulos AP, Keller T. Environmental effects on fatigue behavior of adhesively-bonded pultruded structural joints. Compos Sci Technol 2009;69:1022–8.
[17] Unpublished data from PCI-2 based AE system user's manual. Mistras group.
[18] Kar NK, Barjasteh E, Hu Y, SR Nutt. Bending fatigue of hybrid composite rods. Composites Part: A 2011;42(3):328–36.
[19] Ferreira JAM, Costa JDM, Reis PNB, Richardson MOW. Analysis of fatigue and damage in glass-fibre-reinforced polypropylene composite materials. Compos Sci Technol 1999;59:1461–7.
[20] Harris B. Fatigue Compos, vol. 45–46. CRC Press; 2003. 283.
[21] Curtis PT. Tensile fatigue mechanisms in unidirectional polymer matrix composite materials. Int J Fatigue 1991;13(5):377–82.
[22] Kim HC, Ebert LJ. Fatigue life-limiting parameters in fiberglass composites. J Mater Sci 1979;14:2616–24.
[23] Mandell JF, McGarry FJ, Hsieh AJY, Li CG. Tensile fatigue of glass fibers and composites with conventional and surface compressed fibers. J Polym Compos 1985;6(3):168–74.
[24] Bader MG, Pickering KL, Buzton A, Rezifard A, Smith PA. Failure micromechanisms in continuous carbon-fiber/epoxy-resin composites. Compos Sci Technol 1993;48(1–4):135–42.
[25] Gamstedt EK, Berglund LA, Peijs T. Fatigue mechanisms in unidirectional glass-fibre-reinforced polypropylene. Compos Sci Technol 1999;59:759–68.
[26] Talreja R. Fatigue of composite materials: damage mechanisms and fatigue-life diagrams. Proc R Soc Lond A 1981;378:461–75.
[27] Portnov G, Bakis CE. Analysis of stress concentration during tension of round pultruded composite rods. Compos Struct 2008;83:100–9.
[28] Woldesenbet E. Finite element stress analysis of composite sucker rods. J Energy Resour 2003.
[29] Krishnan A, Xu LR. Effect of the interfacial stress distribution on the material interfacial shear strength measurement. Exp Mech 2009.